Available online at www.sciencedirect.com
SCIENCE DIRECT®
Journal of Magnetic Resonance 159 (2002) 167–174
JMR Journal of Magnetic Resonance
www.academicpress.com

# The effect of Hartmann–Hahn mismatching on polarization inversion spin exchange at the magic angle

Riqiang Fu,[a,*] Changlin Tian,[a,b] Hyeongnam Kim,[a,c] Scott A. Smith,[a] and Timothy A. Cross[a,b,c]

[a] *Center for Interdisciplinary Magnetic Resonance, National High Magnetic Field Laboratory, 1800 E. Paul Dirac Drive, Tallahassee, FL 32310, USA*
[b] *Institute of Molecular Biophysics, Florida State University, Tallahassee, FL 32306, USA*
[c] *Department of Chemistry and Biochemistry, Florida State University, Tallahassee, FL 32306, USA*

Received 23 May 2002; revised 3 August 2002

**Abstract**

The effect of the Hartmann–Hahn mismatch $\Delta = \omega_{eff} - \omega_{1S}$ during polarization inversion spin exchange at the magic angle (PISEMA) has been investigated, where $\omega_{eff}$ and $\omega_{1S}$ represent the amplitudes of the $^1$H effective spin-locking field at the magic angle and the $^{15}$N RF spin-locking field, respectively. During the PISEMA evolution period, the exact Hartmann–Hahn match condition (i.e., $\Delta = 0$) yields a maximum dipolar scaling factor of 0.816 for PISEMA experiments, while any mismatch results in two different effective fields for the first and second half of each frequency switched Lee–Goldburg (FSLG) cycle. The mismatch effect on the scaling factor depends strongly on the transition angle from one effective field to the other within each FSLG cycle as well as on the cycle time. At low RF spin-lock amplitudes in which the FSLG cycle time is relatively long, the scaling factor rapidly becomes smaller as $\omega_{1S}$ becomes greater than $\omega_{eff}$. On the other hand, when $\omega_{1S} < \omega_{eff}$, there is relatively little effect on the scaling factor with variation in $\Delta$. As a result, the presence of RF inhomogeneities may significantly broaden the line-width in the dipolar dimension because of the mismatch effect. Higher RF spin-lock amplitudes result in a relatively small variation for the scaling factor. Furthermore, ramped amplitude of the $^{15}$N RF spin-lock field in synchronization with the flip-flop of the FSLG sequence minimizes the transition angle between the two effective fields within the FSLG cycle. It is shown experimentally that such a ramped amplitude not only gives rise to the same scaling factor but also results in a narrower dipolar line-width in comparison with the rectangular amplitude.


*Keywords:* Frequency switched Lee–Goldburg; PISEMA; Magic angle; Hartmann–Hahn

## 1. Introduction

Polarization inversion spin exchange at the magic angle (PISEMA) [1] has been widely used to obtain orientational constraints from membrane proteins in a lamellar phase lipid environment [2–6]. In PISEMA experiments, a 180° phase shift of the spin-locking field applied to dilute S spins (e.g., $^{15}$N) is synchronous with the phase and frequency alternation in the so-called frequency switched Lee–Goldburg (FSLG) sequence [7], which is applied to abundant I spins (e.g., $^1$H) for suppression of strong proton homonuclear dipolar interactions. Efficient spin exchange between the I and S spins takes place when the two spin-locking fields fulfill the so-called Hartmann–Hahn match condition, i.e., $\omega_{eff} = \omega_{1S}$ [8], where $\omega_{eff} = \gamma_I B_{eff}$ represents the amplitude of the spin-locking field along the magic angle for the I spins while $\omega_{1S} = \gamma_S B_{1S}$ is the RF amplitude applied to the S spins. However, many factors may affect precise calibration of RF spin-locking fields [9] so that it becomes extremely difficult to fulfill an exact Hartmann–Hahn match condition in PISEMA experiments. For instance, the spin-locking fields vary within the sample region because of the RF inhomogeneities across a large rectangular sample coil, which is used to acquire weak NMR signals from aligned samples such as membrane proteins. Amplifier instabilities also provide

* Corresponding author. Fax: 1-850-644-1366.
*E-mail address:* rfu@magnet.fsu.edu (R. Fu).

1090-7807/02/$ - see front matter © 2002 Elsevier Science (USA). All rights reserved.
PII: S1090-7807(02)00036-8

another source for the variation of the RF spin-locking fields, especially for long duration measurements. In particular, for uniformly labeled samples, the chemical shift resonances disperse in a wide range, especially at higher fields, so that the exact Hartmann–Hahn match condition is impossible to fulfill over the wide range of offsets with respect to the RF carrier. Therefore, there is a need to investigate the effect of the Hartmann–Hahn mismatch on the PISEMA spectra.

Cross-polarization (CP) [10] has become a routine technique for signal enhancement of the dilute S spins from the abundant I spins. Many spectroscopic approaches have been proposed in the past decades to enhance the CP efficiency by broadening the Hartmann–Hahn match condition in both static [11–13] and magic angle spinning (MAS) [14–21] NMR. Although both CP and spin exchange are associated with spin polarization transfer, which is governed by heteronuclear dipolar interactions in solids, their foci are fundamentally different. The former aims at an efficient transfer from the I to S spins mainly for signal enhancement, while the latter requires sufficient polarization exchange between the I and S spins allowing us to extract the heteronuclear dipolar interactions. As an example, transient dipolar oscillations resulting from the heteronuclear dipolar interactions were observed during the Hartmann–Hahn CP in systems that exhibit a relatively weak proton–proton coupling network [22,23]. However, by using adiabatic schemes such as adiabatic passage [12] and variable-amplitude [13] CP, signals were greatly enhanced at the price of smoothing out the dipolar oscillations. Therefore, the methods developed for CP may not be necessarily appropriate for spin exchange. So far, PISEMA has been considered the best experiment in terms of resolution and dipolar scaling factor [24] compared to any other methods such as separated-local-field (SLF) with [25,26] and without [27] homonuclear dipolar decoupling for measuring the heteronuclear dipolar couplings in oriented samples.

In this study, the effects of the Hartmann–Hahn mismatch on PISEMA spectra are discussed, including the effects on the dipolar scaling factor, resolution, and intensities of the dipolar oscillation, which are the three major parameters used to characterize the PISEMA experiments. Ramped RF amplitude of the $^{15}$N spin-locking field in synchronization with the flip-flop of the FSLG is further proposed and its effects on the dipolar scaling factor, resolution, and intensities are discussed experimentally in comparison with the rectangular $^{15}$N RF amplitude.

## 2. Theory

Fig. 1a shows the basic pulse sequence for PISEMA experiments. After cross-polarization from abundant I spins (e.g., $^{1}$H) to dilute S spins (e.g., $^{15}$N), the proton magnetization is flipped to the magic angle, along which the polarization inversion spin exchange is established by applying a FSLG sequence to the I spins in synchronization with 180° phase alternations of the spin-locking field applied to the S spins.

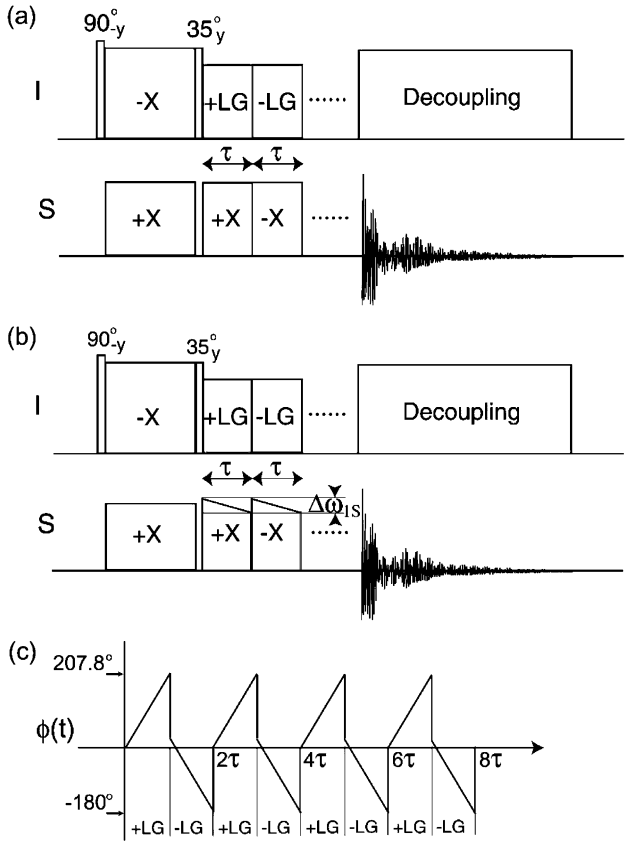


Fig. 1. Pulse sequences for 2D PISEMA experiments with a $t_1$ increment of $2\tau$. (a) The $^{15}$N RF spin-lock amplitude is rectangular. (b) The $^{15}$N RF spin-lock amplitude is ramped. (c) Four cycles of the FSLG sequence achieved by ramping the phase of the $^{1}$H RF spin-lock field.

In a doubly rotating frame synchronized with the Larmor frequencies of $\omega_{0I}$ and $\omega_{0S}$, the spin Hamiltonians during the mixing of the polarization inversion spin exchange for an IS spin pair can be expressed by:

$$H_1 = -\Delta\omega I_Z - \omega_{1I} I_X - \omega_{1S} S_X + 2bI_Z S_Z + H_{II}, \quad (1)$$

$$H_2 = \Delta\omega I_Z + \omega_{1I} I_X + \omega_{1S} S_X + 2bI_Z S_Z + H_{II}, \quad (2)$$

where $H_1$ and $H_2$ represent the Hamiltonians during the first and second half of each FSLG cycle, and $\omega_{1I}$ and $\omega_{1S}$ are the RF amplitudes of the spin-lock fields for the I and S spins, respectively, and $\Delta\omega$ stands for the proton resonance offset, $b$ is the heteronuclear dipolar coupling between the proton and its attached S spin, and $H_{II}$ is the homonuclear dipolar interaction among protons. Here we assume that the RF field of the S spin is applied on-resonance and $b$ dominates any other heteronuclear dipolar interaction between the S spin and other protons. Spin-locking along the magic angle, $\theta_M$, is achieved

by setting the RF amplitude and offset so as to fulfill $\theta_M = \tan(\omega_{1I}/\Delta\omega)$. Thus, an initial spin density before the polarization inversion spin exchange is prepared as

$$\rho(0) = \cos\theta_M I_Z + \sin\theta_M I_X - S_X. \tag{3}$$

After a transformation into a doubly tilted rotating frame by

$$U_1 = \exp[-i\theta_M I_Y]\exp\left[-i\frac{\pi}{2}S_Y\right], \tag{4}$$

the Hamiltonian in Eq. (1) becomes

$$\begin{aligned}\tilde{H}_1 = & -\omega_{eff}I_Z - \omega_{1S}S_Z - 2b\cos\theta_M I_Z S_X \\ & + 2b\sin\theta_M I_X S_X + P_2(\cos\theta_M)H_{II}\end{aligned} \tag{5}$$

with the effective field $\omega_{eff} = \sqrt{\Delta\omega^2 + \omega_{1I}^2}$, and the proton homonuclear dipolar interaction $H_{II}$ is scaled by a factor of $P_2(\cos\theta_M)$. At the magic angle $\theta_M$, we have $P_2(\cos\theta_M) = 0$. In addition, the flip-flop of the FSLG sequence further suppresses the higher order terms in the average homonuclear dipolar Hamiltonian. Thus the last term in Eq. (5) can be dropped in the following evolutions. In this doubly tilted rotating frame, the initial spin density becomes

$$\tilde{\rho}(0) = I_Z - S_Z. \tag{6}$$

A time-dependent transformation of Eq. (5) by the rotation

$$U_2 = \exp\lfloor i\omega_{eff}tI_Z\rfloor\exp[i\omega_{1S}tS_Z] \tag{7}$$

yields the effective Hamiltonian

$$\begin{aligned}\tilde{\tilde{H}}_1 &= U_2\tilde{H}_1U_2^{-1} \\ &= -2b\cos\theta_M(I_ZS_X\cos\omega_{1S}t + I_ZS_Y\sin\omega_{1S}t) \\ &\quad + b\sin\theta_M[(I_XS_X + I_YS_Y)\cos\Delta t - (I_XS_Y - I_YS_X)\sin\Delta t] \\ &\quad + b\sin\theta_M[(I_XS_X - I_YS_Y)\cos\Sigma t - (I_XS_Y + I_YS_X)\sin\Sigma t],\end{aligned} \tag{8}$$

where $\Sigma = \omega_{eff} + \omega_{1S}$, $\Delta = \omega_{eff} - \omega_{1S}$. If we assume that the spin-lock amplitudes on both the I and S spins are much greater than the heteronuclear IS dipolar coupling, i.e., $\omega_{eff}, \omega_{1S} \gg b$, the rapid oscillation terms in Eq. (8) can be dropped from the average Hamiltonian

$$\begin{aligned}\bar{\tilde{\tilde{H}}}_1 = & b\sin\theta_M[(I_XS_X + I_YS_Y)\cos\Delta t \\ & - (I_XS_Y - I_YS_X)\sin\Delta t].\end{aligned} \tag{9}$$

After a rotation by

$$U_3 = \exp\left[-i\Delta t\frac{1}{2}(I_Z - S_Z)\right], \tag{10}$$

the average Hamiltonian in Eq. (9) can be rewritten as

$$\bar{H}_1 = -\Delta\frac{1}{2}(I_Z - S_Z) + b\sin\theta_M(I_XS_X + I_YS_Y). \tag{11}$$

Similarly, after the transformations of $U_1$, $U_2$, and $U_3$, the Hamiltonian of Eq. (2) can be described by an average Hamiltonian in the same frame as in Eq. (11)

$$\bar{H}_2 = \Sigma(I_Z + S_Z) + \Delta\frac{1}{2}(I_Z - S_Z) + b\sin\theta_M(I_XS_X + I_YS_Y). \tag{12}$$

For convenience, we define single-transition operators [15] by, $I_Z^{23} = (I_Z - S_Z)/2$, $I_Z^{14} = (I_Z + S_Z)/2$, and $I_X^{23} = I_XS_X + I_YS_Y$, where (14) and (23) represent the two different subspaces. Because $I_Z^{14}$ always commutes with $I_Z^{23}$ and $I_X^{23}$, the first term in Eq. (12) does not contribute to the spin exchange between the I and S spins. Therefore, the relevant average Hamiltonians in Eqs. (11) and (12) can be rewritten in the same frame by

$$\bar{H}_1 = -\Delta I_Z^{23} + b\sin\theta_M I_X^{23}, \tag{13}$$

$$\bar{H}_2 = \Delta I_Z^{23} + b\sin\theta_M I_X^{23}. \tag{14}$$

In the (23) subspace, the initial density operator $\tilde{\rho}(0) = I_Z - S_Z = 2I_Z^{23}$ because it is not affected by the transformations of $U_2$ and $U_3$. A schematic representation of the average Hamiltonians and the density operator in the (23) subspace is shown in Fig. 2a. Clearly, the mismatch $\Delta$ gives rise to different directions of the average Hamiltonians for the first and second half of the FSLG cycle. The magnetization first rotates through $\beta_1 = \omega_b\tau$ around the axis $\vec{n}_1 = (\cos\varphi, 0, -\sin\varphi)$ and then through the same angle $\beta_1 = \omega_b\tau$ around another axis $\vec{n}_2 = (\cos\varphi, 0, \sin\varphi)$, where

$$\omega_b = \sqrt{\Delta^2 + (b\sin\theta_M)^2}, \tag{15}$$

$$\varphi = \tan^{-1}\left(\frac{\Delta}{b\sin\theta_M}\right). \tag{16}$$

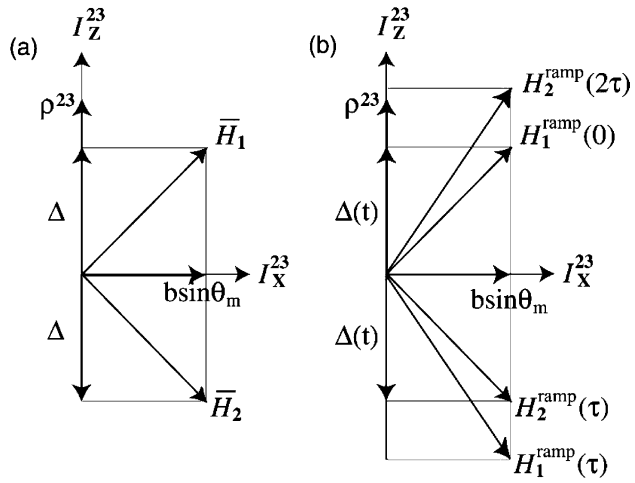


Fig. 2. Schematic representations of Hamiltonians during the mixing of the polarization inversion spin exchange in the (23) subspace, where the spin exchange takes place. In the plots, $b$ represents the heteronuclear dipolar coupling between the I and S spins, $\theta_M$ is the magic angle, and the mismatch parameter $\Delta$ is defined by $\Delta = \omega_{eff} - \omega_{1S}$, where $\omega_{eff}$ and $\omega_{1S}$ are the amplitudes for the $^1$H effective field along the magic angle and the $^{15}$N spin-locking field, respectively. The initial spin density $\rho^{23}$ is along the $+z$ axis. (a) The average Hamiltonians in the first and second half of each FSLG cycle when the $^{15}$N RF amplitude is rectangular. (b) The transient Hamiltonians in the first and second half of each FSLG cycle when the $^{15}$N RF amplitude is ramped.

Thus, the overall behavior of the magnetization in each FSLG period can be described by a single rotation of an angle $\beta_{12}$ around an effective axis $\vec{n}_{12}$, defined as follows [28]:

$$\cos\frac{\beta_{12}}{2} = \cos^2\frac{\beta_1}{2} - \sin^2\frac{\beta_1}{2}\cos 2\varphi, \tag{17}$$

$$\sin\frac{\beta_{12}}{2}\vec{n}_{12} = \cos\frac{\beta_1}{2}\sin\frac{\beta_1}{2}(\vec{n}_1 + \vec{n}_2) - \sin^2\frac{\beta_1}{2}\vec{n}_1 \times \vec{n}_2. \tag{18}$$

Therefore, we have:

$$\vec{n}_{12} = (\cos\gamma, -\sin\gamma, 0), \tag{19}$$

$$\cos\beta_{12} = \cos^4\varphi\cos 2\beta_1 + \sin^2 2\varphi\cos\beta_1 - \sin^2\varphi(\cos 2\varphi + \cos^2\varphi), \tag{20}$$

where $\gamma = \tan^{-1}(\tan(\beta_1/2)\sin\varphi)$. From Eq. (19), we know that the effective axis $\vec{n}_{12}$ for the FSLG period always lies on the $x$–$y$ plane in the (23) subspace. Therefore, spin exchange can take place even if the mismatch $\Delta$ is considerably larger than the dipolar coupling $b$ [11], which was observed experimentally (spectra not shown). Since the spin exchange between the I and S spins is described by $\cos\beta_{12}$, where $\beta_{12} = 2n\tau\omega_{12}$, the processional frequency $\omega_{12}$ depends not only on the transition angle, which is the angle between the two effective fields $\overline{H}_1$ and $\overline{H}_2$ within FSLG cycles, but also on the rotation angle $\beta_1$. The last term in Eq. (20) depends only on the transition angle and thus results in artifacts at zero-frequency. A dipolar scaling factor is defined by $\omega_{12}/b$. Fig. 3a shows a simulated plot of the dipolar scaling factor and the peak intensity versus $\Delta/b$, assuming $\omega_{\text{eff}} = 40\,\text{kHz}$ and $b = 14.8\,\text{kHz}$. A maximum scaling factor is obtained at the exact Hartmann–Hahn match condition. As is evident, the scaling factor decreases dramatically with an increase of the mismatch if $\omega_{1S} > \omega_{\text{eff}}$. On the other hand, the change in the scaling factor is relatively small with the mismatch at $\omega_{1S} < \omega_{\text{eff}}$. In fact, this can be understood by two extreme cases. (1) When $\omega_{1S} = 0$, the FSLG sequence on the I spins acts as homonuclear decoupling so that the heteronuclear dipolar coupling is scaled by $\cos\theta_M$ [1]. (2) When $\omega_{1S} \gg \omega_{\text{eff}}$ the S spins are strongly spin-locked so that the scaling factor becomes zero. In addition, when the rotation angle $\beta_1 = 2\pi$, the net process by the effective fields $\overline{H}_1$ and $\overline{H}_2$ is null, as if the $^{15}$N magnetization is perfectly spin-locked, thus yielding a zero scaling factor, as indicated in Fig. 3a when $\Delta/b = -2.7$ (i.e., $\Delta = 40\,\text{kHz}$). When $\omega_{\text{eff}}$ is doubled to 80 kHz, the processional time $\tau$ is shortened by a factor of two so that the rotation angle $\beta_1$ becomes half of that under the same mismatch condition when $\omega_{\text{eff}} = 40\,\text{kHz}$. Fig. 3b shows the simulated plot of the scaling factor and the intensity of the dipolar splitting versus $\Delta/b$ at $\omega_{\text{eff}} = 80\,\text{kHz}$. Clearly, the scaling factor becomes less sensitive to the mismatch $\Delta$ at higher RF spin-lock amplitudes at the expense of proton spin-locking efficiency [29].

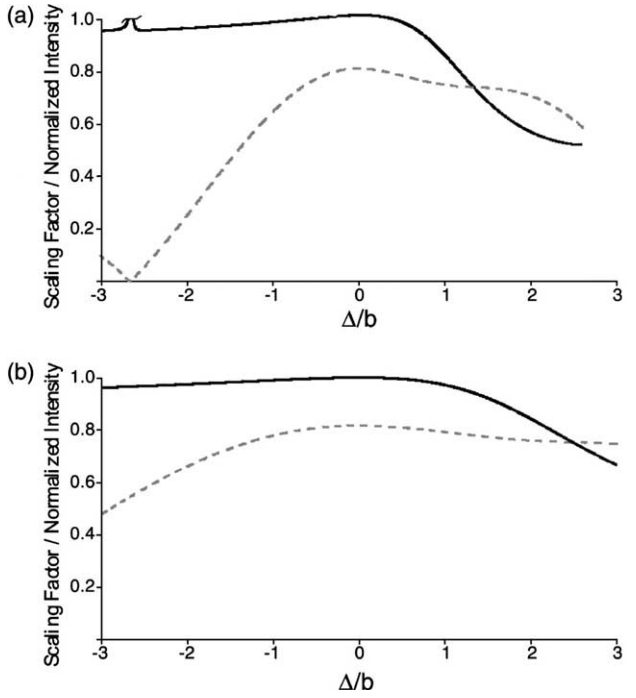


Fig. 3. Plots of the dipolar scaling factor and normalized intensity of the dipolar splitting versus the ratio of the mismatch parameter $\Delta$ over the dipolar coupling $b$ for different RF spin-lock amplitudes, where $\Delta = \omega_{\text{eff}} - \omega_{1S}$. The scaling factor is indicated by the dashed lines and the intensity by the solid lines, which is normalized to that at the exact matching condition (i.e., $\Delta = 0$). (a) $\omega_{\text{eff}} = 40\,\text{kHz}$. (b) $\omega_{\text{eff}} = 80\,\text{kHz}$. The GAMMA magnetic resonance simulation platform [34] was used for the simulations, in which $b$ was set to 14.8 kHz for an isolated two-spin system and $\omega_{1S}$ was varied correspondingly.

In analogy to the case of the rectangular $^{15}$N spin-locking field, when the $^{15}$N RF amplitude is ramped in synchronization with the FSLG sequence, as shown in Fig. 1b, the average Hamiltonians in the first and second half of each FSLG cycle can be described in the (23) subspace as,

$$\overline{H}_1^{\text{ramp}} = -\int_0^{\tau}\Delta(t)\,dt\,I_Z^{23} + b\sin\theta_M I_X^{23}, \tag{21}$$

$$\overline{H}_2^{\text{ramp}} = \int_{\tau}^{2\tau}\Delta(t)\,dt\,I_Z^{23} + b\sin\theta_M I_X^{23}, \tag{22}$$

where the mismatch $\Delta(t) = \omega_{\text{eff}} - \omega_{1S}(t)$ becomes time-dependent. Fig. 2b shows the schematic representation of the transient Hamiltonians in the (23) subspace. At the beginning of the first half cycle, the Hamiltonian $H_1^{\text{ramp}}$ is positioned in the $+x+z$ plane, provided $\omega_{1S}(0) > \omega_{\text{eff}}$. As the amplitude ramps from $\omega_{1S}(0)$ to $\omega_{1S}(\tau)$ (provided $\omega_{1S}(\tau) < \omega_{\text{eff}}$), $H_1^{\text{ramp}}$ crosses over the $x$-axis and moves into the $+x-z$ plane, in which the Hamiltonian $H_2^{\text{ramp}}$ is located at the beginning of the

second half cycle. Similarly, $H_2^{\text{ramp}}$ moves from the $+x-z$ into $+x+z$ plane as the amplitude ramps from $\omega_{1S}(0)$ to $\omega_{1S}(\tau)$. As a result, the transition angle between $H_1^{\text{ramp}}(\tau)$ and $H_2^{\text{ramp}}(\tau)$, and $H_2^{\text{ramp}}(2\tau)$ and $H_1^{\text{ramp}}(0)$ could become much smaller compared to that between $\overline{H}_1$ and $\overline{H}_2$ as in Fig. 2a.

## 3. Materials and experiments

Gramicidin A (gA) is a polypeptide of 15 amino acid residues, whose high-resolution structure in lipid bilayers has been uniquely defined using 120 orientational restraints from solid-state NMR [30,31]. Here [$^{15}$N]Leu$_4$ labeled gramicidin A was used. The oriented gA sample was prepared by codissolving 10-mg gA and 30-mg dimyristoylphosphatidylcholine (DMPC) in 1.5 ml 95/5 (v/v) benzene/ethanol solution. Thirty μl of the solution was spread on each of 50 glass slides ($5.7 \times 12.0 \times 0.07\,\text{mm}^3$), following which the solvents were partially evaporated in air at room temperature. Drying was completed overnight in a vacuum. These glass slides were then stacked in a square glass tube ($6.0 \times 6.0 \times 15.0\,\text{mm}^3$). The tube was sealed after adding 50% HPLC-grade $H_2O$ (by total sample dry weight) and incubated at 43 °C until the sample became transparent and uniformly hydrated. The sample was placed in the magnetic field such that the normal to the lipid bilayers was parallel to $B_0$.

All NMR measurements were carried out at 43 °C on a 400-MHz NMR spectrometer with a DRX console, equipped with a home-built wideline $^1$H–$^{15}$N double resonance NMR probe using a large rectangular sample coil ($8 \times 8 \times 12\,\text{mm}^3$). The coil was directly wound on the sample tube using a copper foil tape in order to enhance the RF performance of the probe [32]. The Larmor frequencies of $^1$H and $^{15}$N are 400.1 and 40.5 MHz, respectively. The $^{15}$N signals of the oriented [$^{15}$N]Leu$_4$ gA sample was enhanced by optimizing Hartmann–Hahn matching condition. The $^{15}$N RF spin-lock amplitude of 47.6 kHz used in the CP was determined via the measurement of 180° pulse-length, while the matching $^1$H RF spin-lock amplitude was calibrated to be 45.5 kHz experimentally by the measurement of $^1$H 180° pulse-length via indirect observation of the $^{15}$N signals through CP. After conventional CP, $^{15}$N magnetization was enhanced while the $^1$H magnetization was flipped to the magic angle, followed by the sequences used for polarization inversion spin exchange, as shown in Fig. 1. In order to maintain the Hartmann–Hahn match condition during the PISEMA spin exchange period, the $^1$H RF amplitude was decreased to 37.1 kHz, which was also experimentally calibrated, so that the effective field along the magic angle was still 45.5 kHz. For each cycle, FSLG was achieved by sweeping the phase of the spin-locking field linearly from 0° to 207.8° for 22 μs (the first half of each FSLG cycle) and then from 27.8° to −180° for another 22 μs (the second half of the cycle). Thus the $t_1$ increment was 44 μs yielding a dipolar spectral width of 22.73 kHz in the resulting two-dimensional (2D) PISEMA spectra. Fig. 1c shows four cycles of the FSLG sequence. In our experiments, $n$ cycles of the FSLG sequence were programmed into a waveform to avoid any time interval between FSLG cycles in pulse programs. A similar waveform was generated for the $^{15}$N spin-locking field with constant phases of 0° and 180° for the first and second half of each cycle, respectively. The ramped RF amplitude shown in Fig. 1b was programmed in the waveform. The two waveforms were then applied simultaneously to the $^1$H and $^{15}$N channels, respectively, for the $n$th $t_1$ increment of 2D PISEMA spectra. For each $t_1$ increment, 200 scans were recorded to accumulate the $^{15}$N signals with a recycle delay of 6 s. A total of $64t_1$ increments were recorded and zero-filled to 1024 points before Fourier transform.

## 4. Results and discussion

The $^1$H–$^{15}$N dipolar coupling of the oriented gA sample was obtained through the SLF measurement [27]. In such an oriented sample, $^{15}$N signals were observed at 145 ppm with respect to 0 ppm for a saturated solution of $^{15}NH_4NO_3$ [30]. Fig. 4a shows a slice taken at 145 ppm along the dipolar dimension of a 2D SLF spectrum. Because the SLF experiment does not scale the heteronuclear dipolar interaction, the dipolar splitting of 14.8 kHz observed here represents the unscaled $^1$H–$^{15}$N dipolar coupling. Similarly, Fig. 4b shows a slice taken at 145 ppm along the dipolar dimension of the 2D PISEMA spectrum recorded using the sequence of Fig. 1a with a $^{15}$N RF amplitude of 47.6 kHz. With the $^1$H effective RF amplitude of 45.5 kHz along the magic angle, the $^{15}$N RF amplitude approximately fulfilled the Hartmann–Hahn condition during the mixing. Obviously, the spectral resolution in the dipolar dimension of the PISEMA spectrum is significantly better than that of the SLF spectrum. As shown in Fig. 4b, the observed dipolar splitting is 11.8 kHz, yielding a dipolar scaling factor of 0.80, slightly smaller than the theoretical value of 0.816. It is worth noting from Fig. 4b that, in addition to the dipolar splitting, there is a negative peak at zero-frequency. The zero-frequency component could result from the imperfect preparation of the spins' states before the spin exchange mixing, the Hartmann–Hahn mismatch, and/or proton spin-diffusion. When the $^{15}$N RF amplitude was decreased to 33.0 kHz, the Hartmann–Hahn mismatch condition was imposed during the mixing. Under this mismatch condition, the resulting dipolar splitting becomes 10.6 kHz, as shown in Fig. 4c, yielding a dipolar scaling factor of 0.72. As can be no-

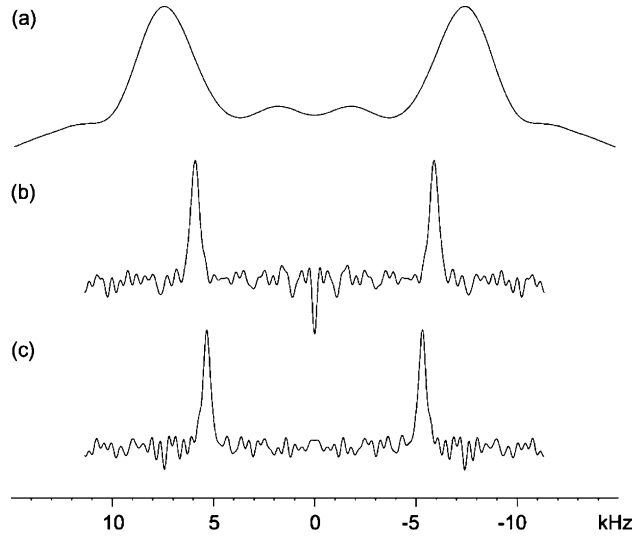


Fig. 4. Dipolar spectra of [$^{15}$N]Leu$_4$ gA oriented in DMPC (1:8 molar ratio) bilayers taken at 145 ppm along the dipolar dimension of the 2D dipolar-chemical shift correlation spectra. For PISEMA experiments, the $^1$H RF amplitude was 45.5 kHz for cross-polarization and 37.1 kHz for the polarization inversion spin exchange, while $\tau$ was set to 22 μs corresponding to a $2\pi$-rotation about the magic angle. (a) A slice from the SLF spectrum, where the unscaled heteronuclear dipolar coupling of 14.8 kHz is observed. (b) A slice from the PISEMA spectrum with the $^{15}$N RF amplitude $\omega_{1S} = 47.6$ kHz, in which the dipolar splitting is 11.8 kHz, yielding a scaling factor of 0.80. A line-width of 510 Hz is measured. (c) A slice from the PISEMA spectrum with $\omega_{1S} = 33.0$ kHz, where the dipolar splitting is 10.6 kHz, resulting in a scaling factor of 0.72 and a line-width of 443 Hz.

ticed in Fig. 4c, the signal intensities are slightly smaller (~2%) while the dipolar line-width is relatively narrow compared to that in Fig. 4b. Interestingly, the zero-frequency component is not visible at the severe mismatch condition. This could be the result of artifacts from the severe mismatch causing cancellation of the negative component that appears in Fig. 4b. However, it is not clear why the line-width becomes narrower under the mismatch condition. A possible explanation is a consequence of the RF inhomogeneities across the sample volume. For instance, for an averaged $^{15}$N spin-lock amplitude of 47.6 kHz, the RF amplitude [33] was larger at some positions (such as close to the sample coil) while less at others (such as further away from the coil) than the effective $^1$H spin-locking amplitude at the magic angle. As can be seen from Fig. 3a, the dipolar scaling factor is not symmetric to the mismatch parameter Δ. In other words, the same mismatch parameter $|\Delta|$ with the larger $^{15}$N spin-lock amplitude gives rise to a smaller dipolar scaling factor compared to the smaller $^{15}$N spin-lock amplitude. As a result, the superimposed dipolar splitting under various mismatch parameters will produce a broader observed line-width. On the other hand, when the averaged $^{15}$N spin-lock amplitude was decreased to 33.0 kHz, the RF amplitude at all positions within the sample coil might be less than 45.5 kHz so that the distribution of the resulting dipolar scaling factor becomes relatively small (cf. Fig. 3a). Consequently, the dipolar line-width becomes relatively narrow. Our simulations (spectra not shown) by using the GAMMA magnetic resonance platform [34] confirm this observation when the RF inhomogeneity is taken into account.

Fig. 5 shows dipolar spectra taken at 145 ppm along the dipolar dimension of the PISEMA spectra recorded by using the sequence shown in Fig. 1b with different $^{15}$N ramped amplitudes. In these experiments, all of the experimental parameters associated with the $^1$H frequency were kept unchanged. As shown in Fig. 5a (same as Fig. 4b), when the depth of the ramped amplitude is $\Delta\omega_{1S} = 0$, the dipolar splitting of 11.8 kHz is observed, resulting in a dipolar scaling factor of 0.80, and the dipolar line-width at half-height is 510 Hz. When the $^{15}$N RF amplitude is ramped from 47.6 to 39.0 kHz, i.e., $\Delta\omega_{1S} = 8.6$ kHz, the resulting dipolar splitting is again 11.8 kHz, as shown in Fig. 5b, thus generating the same dipolar scaling factor of 0.80 as in the PISEMA experi-

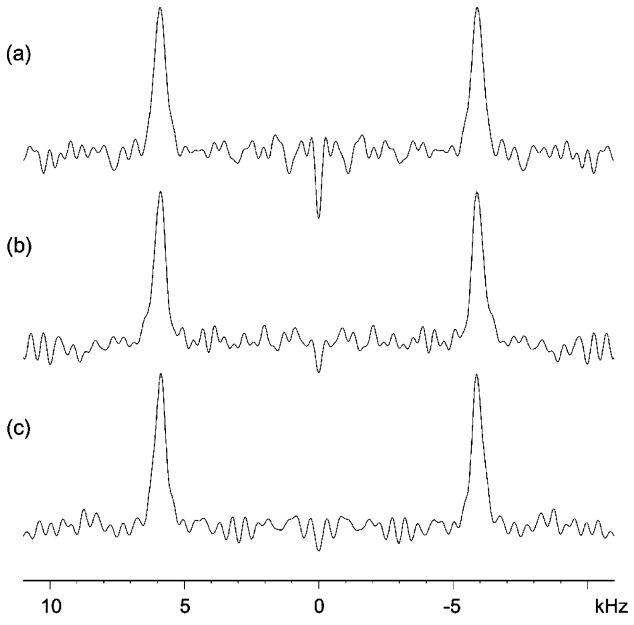


Fig. 5. Dipolar spectra of [$^{15}$N]Leu$_4$ gA oriented in DMPC (1:8 molar ratio) bilayers taken at 145 ppm along the dipolar dimension of the 2D PISEMA spectra. The experimental parameters associated with the $^1$H frequency were the same as in Fig. 4. (a) A slice from the PISEMA spectrum with the $^{15}$N RF amplitude $\omega_{1S}(0) = 47.6$ kHz and $\Delta\omega_{1S} = 0$, (same as Fig. 4b), in which the dipolar splitting is 11.8 kHz, yielding a scaling factor of 0.80. A line-width of 510 Hz was measured. (b) A slice from the PISEMA spectrum with the $^{15}$N RF amplitude ramped from $\omega_{1S}(0) = 47.6$ kHz to $\omega_{1S}(\tau) = 39.6$ kHz (i.e., $\Delta\omega_{1S} = 8.6$ kHz), resulting in an observed dipolar splitting of 11.8 kHz, thus a scaling factor of 0.80. The line-width was 488 Hz, while the signal intensities were about 7% higher compared to (a). (c) A slice from the PISEMA spectrum with the $^{15}$N RF amplitude ramped from $\omega_{1S}(0) = 47.6$ kHz to $\omega_{1S}(\tau) = 33.0$ kHz (i.e., $\Delta\omega_{1S} = 14.6$ kHz). In this spectrum, the observed dipolar splitting was again 11.8 kHz, yielding a scaling factor of 0.80. While the line-width is 466 Hz and the signal intensities are again about 7% higher in comparison with that in (a).

ment with constant $^{15}N$ RF amplitude. Furthermore, the peak maximum in Fig. 5b is about 7% higher than that in Fig. 5a. When the $^{15}N$ RF amplitude is ramped further from 47.6 to 33.0 kHz, i.e., $\Delta\omega_{1S} = 14.6$ kHz, once again the observed dipolar splitting is 11.8 kHz, as shown in Fig. 5c. As in Fig. 5b, the peak maximum in Fig. 5c is increased by about 7% compared with that in Fig. 5a. Therefore, the amplitude ramp in the $^{15}N$ spin-locking field does not affect the resulting dipolar scaling factor experimentally, though our simulations indicate that any mismatch may result in a smaller scaling factor. Once again, it is believed that the discrepancy might result partly from the significant RF inhomogeneities across the sample volume, especially when an unbalanced RF circuit is used as in our probe. Fig. 6 shows simulated dipolar spectra using the PISEMA sequence with $^{15}N$ ramped amplitude, as in Fig. 1b, in the presence of the RF inhomogeneity. It can be seen from Fig. 6 that when the depth of the ramp is increased from 0 to 8.6 kHz, the maximum peak intensities increase along with a decrease in line-width. However, the observed dipolar splitting, thus the scaling factor, does not change (cf. Figs. 6a and b). When the depth of the ramp reaches 14.6 kHz, the maximum peak intensities becomes smaller than that in Fig. 6b, but still larger compared to that in Fig. 6a. However, the scaling factor becomes slightly smaller compared with that in Figs. 6a and b. It is worth noting that these simulations can only roughly demonstrate RF inhomogeneity effects since we have no detailed knowledge of the RF inhomogeneity across the large volume of the sample. Indeed, it can be noticed from Fig. 5 that the dipolar line-width at half-height is steadily decreased as the depth of the ramped amplitude is increased. For the constant $^{15}N$ RF amplitude, various mismatch conditions give rise to different dipolar scaling factors and each of the dipolar splittings by these various mismatch conditions is superimposed so that the dipolar line-width becomes broader (cf. Fig. 5a). However, with the ramped amplitude, the dipolar scaling factor is less sensitive to the mismatch condition so that the dipolar line-width becomes narrower (cf. Figs. 5b and c). It is also interesting to note from Fig. 5 that the signal intensity at zero-frequency becomes smaller when the ramped amplitude is applied to the $^{15}N$ nuclei, which is not predicted by the simulations, as shown in Fig. 6. It is speculated that relaxation might play a role in the minimization of the artifacts at zero-frequency under the PISEMA sequence with $^{15}N$ ramped amplitude, particularly since the gA peptide in the hydrated DMPC lipid bilayers experiences a significant degree of dynamics [35].

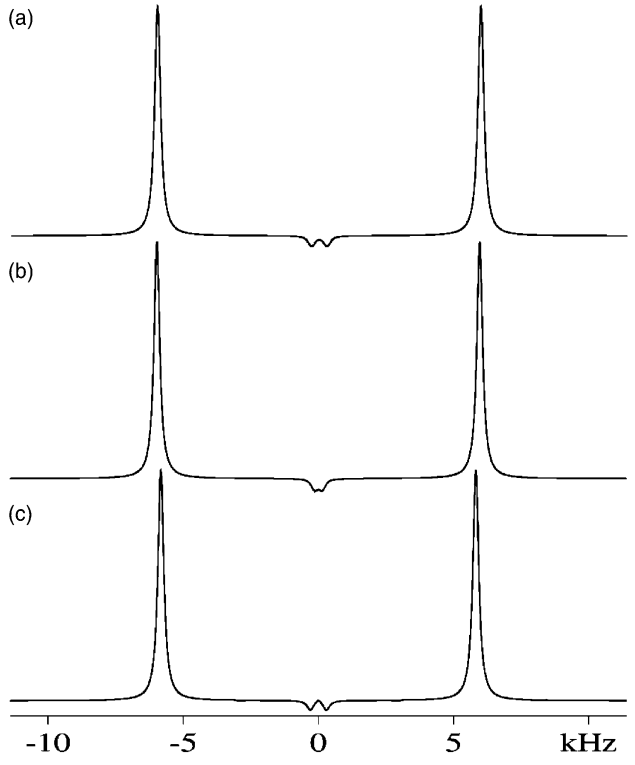


Fig. 6. GAMMA simulated dipolar spectra using the PISEMA sequence with $^{15}N$ ramped amplitude, as in Fig. 1b, in the presence of the RF inhomogeneity. The depth of the ramped amplitudes is: (a) $\Delta\omega_{1S} = 0$. (b) $\Delta\omega_{1S} = 8.6$ kHz. (c) $\Delta\omega_{1S} = 14.6$ kHz. In these simulations, $b$ was set to 14.8 kHz for an isolated two-spin system and $\omega_{1H}$ to 45.5 kHz. For simplicity, we assume here that the RF inhomogeneity applies only to the $^{15}N$ channel across the sample region.

## 5. Conclusion

The Hartmann–Hahn mismatch effect on PISEMA has been discussed theoretically and experimentally. The dipolar scaling factor is very sensitive to the amplitudes of the two RF spin-lock fields as well as the mismatch parameter $\Delta = \omega_{eff} - \omega_{1S}$. The exact Hartmann–Hahn matching condition (i.e., $\Delta = 0$) yields a maximum scaling factor of 0.816 for PISEMA experiments. When the two RF spin-lock amplitudes are relatively weak as in our experiments due to the limitation of the NMR probe, the scaling factor rapidly becomes smaller with an increase of the mismatch when $\omega_{1S} > \omega_{eff}$. On the other hand, the scaling factor has a relatively small variation when $\omega_{1S} < \omega_{eff}$. Consequently, in addition to other line-broadening mechanisms [29,36], the line-width in the dipolar dimension of the PISEMA spectrum may be broadened due to the contribution from the different mismatch condition across a large sample volume in the presence of the RF inhomogeneities. Higher RF spin-lock amplitudes (i.e., shorter processional time) considerably decrease such a mismatch effect on the scaling factor (cf. Fig. 3b) and thus could result in minimization of the dipolar line-broadening due to the RF inhomogeneities. However, it is technically difficult when using an NMR probe with a large sample coil to generate higher $^{15}N$ RF amplitude because of its low gyromagnetic ratio. In addition, the

ramped amplitude of the $^{15}N$ spin-locking field, in synchrony with the flip-flop of the FSLG sequence, has been demonstrated in the PISEMA experiments. It has been shown that, in the presence of the RF inhomogeneities, the ramped amplitude not only gives rise to the same scaling factor, but also results in a narrower linewidth in comparison with the rectangular amplitude.

## Acknowledgments

Authors are indebted to our RF engineers P. Gor'kov and Dr. W.W. Brey in the NMR program for designing the copper foil coils to enhance the probe performance. This work was supported by the National Science Foundation MCB 9986036 and the work was performed at the National High Magnetic Field Laboratory supported by the National Science Foundation Cooperative Agreement DMR-0084173 and the State of Florida.

## References

[1] C.H. Wu, A. Ramamoorthy, S.J. Opella, High-resolution heteronuclear dipolar solid-state NMR spectroscopy, J. Magn. Reson. A 109 (1994) 270–272.
[2] F.M. Marassi, A. Ramamoorthy, S.J. Opella, Complete resolution of the solid-state NMR spectrum of a uniformly $^{15}N$-labeled membrane protein in phospholipid bilayers, Proc. Natl. Acad. Sci. USA 94 (1997) 8551–8556.
[3] Y. Kim, K. Valentine, S.J. Opella, S.L. Schendel, W.A. Cramer, Solid-State NMR studies of the membrane-bound closed state of the colicin E1 channel domain in lipid bilayers, Protein Sci. 7 (1998) 342–348.
[4] F.M. Marassi, S.J. Opella, NMR structural studies of membrane proteins, Curr. Opin. Struct. Biol. 8 (1998) 640–648.
[5] S.J. Opella, F.M. Marassi, J.J. Gesell, A.P. Valente, Y. Kim, M. Oblatt-Montal, M. Montal, Structures of M2 channel-lining segments from nicotinic acetylcholine and NMDA receptors by NMR spectroscopy, Nat. Struct. Biol. 6 (1999) 374–379.
[6] Z. Song, F. Kovacs, J. Wang, J. Denny, S.C. Shekar, J.R. Quine, T.A. Cross, Transmembrane domain of M2 protein from influenza A virus studied by solid-state $^{15}N$ polarization inversion spin exchange at magic angle NMR, Biophys. J. 79 (2000) 767–775.
[7] A. Bielecki, A.C. Kolbert, H.J.M. de Groot, R.G. Griffin, M.H. Levitt, Frequency-switched Lee–Goldburg sequences in solids, Advan. Magn. Reson. 14 (1990) 111–150.
[8] S.R. Hartmann, E.L. Hahn, Nuclear double resonance in the rotating frame, Phys. Rev. 128 (1962) 2042–2053.
[9] K. Nishimura, R. Fu, T.A. Cross, The effect of RF inhomogeneity on heteronuclear dipolar recoupling in solid state NMR: practical performance of SFAM and REDOR, J. Magn. Reson. 152 (2001) 227–233.
[10] A. Pines, M.G. Gibby, J.S. Waugh, Proton-enhanced NMR of dilute spins in solids, J. Chem. Phys. 59 (1973) 569–590.
[11] M.H. Levitt, D. Suter, R.R. Ernst, Spin dynamics and thermodynamics in solid-state NMR cross polarization, J. Chem. Phys. 84 (1986) 4243–4255.
[12] S. Hediger, B.H. Meier, N.D. Kurur, G. Bodenhausen, R.R. Ernst, NMR cross polarization by adiabatic passage through the Hartmann Hahn condition (APHH), Chem. Phys. Lett. 223 (1994) 283–288.
[13] S. Zhang, Quasi-adiabatic polarization transfer in solid-state NMR, J. Magn. Reson. A 110 (1994) 73–76.
[14] T.M. Barbara, E.H. Williams, Modulated sequences for cross polarization during high-speed MAS, J. Magn. Reson. 99 (1992) 439.
[15] X. Wu, K.W. Zilm, Cross polarizaton with high-speed magic-angle spinning, J. Magn. Reson. A 104 (1993) 154.
[16] S. Hediger, B.H. Meier, R.R. Ernst, Cross polarization under fast magic angle sample spinning using amplitude-modulated spin-lock sequences, Chem. Phys. Lett. 213 (1993) 627–635.
[17] S. Hediger, B.H. Meier, R.R. Ernst, Rotor-synchronized amplitude-modulated nuclear magnetic resonance spin-lock sequences for improved cross polarization under fast magic angle sample spinning, J. Chem. Phys. 102 (1995) 4000–4011.
[18] O.B. Peersen, X. Wu, I. Kustanovich, S.O. Smith, Variable-amplitude cross polarization MAS NMR, J. Magn. Reson. A 104 (1993) 334–339.
[19] G. Metz, X. Wu, S.O. Smith, Ramped-amplitude cross polarization in magic-angle-spinning NMR, J. Magn. Reson. A 110 (1994) 219–227.
[20] A.C. Kolbert, A. Bielecki, Broadband Hartmann–Hahn matching in magic-angle spinning NMR via an adiabatic frequency sweep, J. Magn. Reson. A 116 (1995) 29–35.
[21] R. Fu, P. Pelupessy, G. Bodenhausen, Frequency-modulated cross-polarization for fast magic angle spinning NMR at high field: relaxing the Hartmann–Hahn condition, Chem. Phys. Lett. 264 (1997) 63–69.
[22] L. Müller, A. Kumar, T. Baumann, R.R. Ernst, Transient oscillations in NMR cross-polarization experiments in solids, Phys. Rev. Lett. 32 (1974) 1402–1406.
[23] F. Tian, T.A. Cross, Dipolar oscillations in cross-polarized peptide samples in oriented lipid bilayers, J. Magn. Reson. 125 (1997) 220–223.
[24] A. Ramamoorthy, S.J. Opella, Experimental aspects of multidimensional solid-state NMR correlation spectroscopy, J. Magn. Reson. 140 (1999) 131–140.
[25] W.K. Rhim, D.D. Elleman, R.W. Vaughan, Enhanced resolution for solid state NMR, J. Chem. Phys. 58 (1973) 1772.
[26] M. Lee, W. Goldburg, Nuclear magnetic resonance line narrowing by a rotating RF field, Phys. Rev. 140 (1965) 1261–1271.
[27] J.S. Waugh, Uncoupling of local field spectra in nuclear magnetic resonance: determination of atomic positions in solids, Proc. Natl. Acad. Sci. USA 73 (1976) 1394–1397.
[28] C. Counsell, M.H. Levitt, R.R. Ernst, Analytical theory of composite pulses, J. Magn. Reson. 63 (1985) 133–141.
[29] R. Fu, C. Tian, T.A. Cross, NMR spin locking of proton magnetization under frequency switched Lee–Goldburg (FSLG) pulse sequence, J. Magn. Reson. 154 (2002) 130–135.
[30] R. Ketchem, W. Hu, T.A. Cross, High-resolution conformation of gramicidin A in a lipid bilayer by solid state NMR, Science 261 (1993) 1457–1460.
[31] R.R. Ketchem, B. Roux, T.A. Cross, High-resolution polypeptide structure in a lameller phase lipid environment from solid state NMR derived orientational constraints, Structure 5 (1997) 1655–1669.
[32] W.W. Brey, P.L. Gor'kov, C. Tian, R. Fu, T.A. Cross, Improvements in NMR probes for membrane protein studies, 43rd ENC, 2002.
[33] W.W. Brey, Rf inhomogeneity in NMR spectroscopy at high field, 41st ENC, 2000.
[34] S.A. Smith, T.O. Levante, B.H. Meier, R.R. Ernst, Computer stimulations in magnetic resonance. An object oriented job approach., J. Magn. Reson. A 106 (1994) 75–105.
[35] C.L. North, T.A. Cross, Correlations between function and dynamics: time scale coincidence for ion translocation and molecular dynamics in the gramicidin channel backbone, Biochemistry 34 (1995) 5883–5895.
[36] Z. Gan, Spin dynamics of polarization inversion spin exchange at the magic angle in multiple spin systems, J. Magn. Reson. 143 (2000) 136–143.